Isomerization and Decomposition Reactions in the Pyrolysis of Branched Hydrocarbons: 4-Methyl-1-pentyl Radical

W. Sean McGivern,* Iftikhar A. Awan, Wing Tsang, and Jeffrey A. Manion

Physical and Chemical Properties Division, National Institute of Standards and Technology, 100 Bureau Drive Stop 8380, Gaithersburg, Maryland 20899-8380

Received: March 6, 2008; Revised Manuscript Received: May 14, 2008

The kinetics of the decomposition of 4-methyl-1-pentyl radicals have been studied from 927−1068 K at pressures of 1.78−2.44 bar using a single pulse shock tube with product analysis. The reactant radicals were formed from the thermal C−I bond fission of 1-iodo-4-methylpentane, and a radical inhibitor was used to prevent interference from bimolecular reactions. 4-Methyl-1-pentyl radicals undergo competing decomposition and isomerization reactions via β-bond scission and 1,x-hydrogen migrations ($x = 4, 5$), respectively, to form short-chain radicals and alkenes. Major alkene products, in decreasing order of concentration, were propene, ethene, isobutene, and 1-pentene. The observed products are used to validate a RRKM/master equation (ME) chemical kinetics model of the pyrolysis. The presence of the branched methyl moiety has a significant impact on the observed reaction rates relative to analogous reaction rates in straight-chain radical systems. Systems that result in the formation of substituted radical or alkene products are found to be faster than reactions that form primary radical and alkene species. Pressure-dependent reaction rate constants from the RRKM/ME analysis are provided for all four H-transfer isomers at 500−1900 K and 0.1−1000 bar pressure for all of the decomposition and isomerization reactions in this system.

Introduction

Aliphatic hydrocarbons make up a substantial portion of liquid combustion fuels and are utilized extensively in surrogate fuel mixtures.[1] Unimolecular reactions of these compounds and radicals derived from the loss of an H-atom provide a significant source of short-chain radicals and olefinic species in typical combustion systems. These compounds undergo further unimolecular and bimolecular reactions and may form unsaturated five- and six-membered ring compounds. Continued reaction of these ring systems with small radical species leads to polycyclic aromatic hydrocarbons (PAHs), finally terminating with particulate soot.[2]

Prior work in our laboratory has established the reactivity of straight-chain hydrocarbon radicals through n-C_6H_{13}.[3,4] Presently, we focus on the thermal decomposition of a branched hydrocarbon radical, 4-methyl-1-pentyl. As in the straight-chain system, the primary reactions of these radicals are decomposition through β-bond scission and isomerization via H-atom transfer through cyclic transition states. However, the system studied presently involves the abstraction of H from a tertiary carbon, which is not present in the straight-chain system. Comparison of the present results with the kinetics of straight-chain hydrocarbon radical pyrolysis will illustrate the effects of methyl substitution and provide insight into the reactions that are important in the pyrolysis of branched hydrocarbons. Such information is necessary to derive generalized rate expressions that describe the reactions for the wide variety of species present in hydrocarbon fuels and their surrogates. The results of shock tube decomposition studies of 4-methyl-1-pentyl radical are used to develop an RRKM/master equation model that permits the calculation of rate constants for the reactivity of branched hydrocarbon species with a radical center near a tertiary carbon for a wide range of temperature and pressures.

A mechanism for the unimolecular decomposition of 4-methyl-1-pentyl radical, showing both the decomposition and isomerization pathways, is shown in Figure 1. Rather than utilizing IUPAC nomenclature for the initial radical species, we have elected to identify the radical isomers as x-4MeP, where x is the position of the radical relative to that in the initial reactant. The use of "4MeP" to identify the backbone emphasizes that the present numbering system considers the methyl to be substituted at the "4" position for all of the radical isomers. The radical numbering scheme and abbreviations used in the present work are shown in the figure.

Experimental Section

The experimental apparatus has been described in detail previously,[6–8] and only a brief overview will be provided.[5] A single pulse shock tube was used to shock heat a mixture of 100 parts per million (ppm) 1-iodo-4-methylpentane (GFS Chemicals, Columbus, OH; no impurities observed by gas chromatography), 1.5% m-xylene (Aldrich, 99+%), and 100 ppm chlorocyclohexene (Aldrich, 99%) in argon (Praxair, 99.999%). After the shock heating and subsequent cooling, which is equivalent to a 500 μs pulsed heater in the present system, the end product spectrum was measured using gas chromatography (GC) with simultaneous flame-ionization (FI) and mass spectrometric (MS) detection. A large excess of m-xylene was added as a radical scavenger; H-atoms in the system react with m-xylene through either abstraction of a methyl hydrogen to form 3-methylbenz-1-yl radicals, which are stable on the experimental time scale, or addition and subsequent displacement of a methyl radical to form toluene. The branching ratios for similar reactions have been measured[9,10] with the ratio of abstraction to displacement, $k_{abs}/k_{disp} \approx 2$. Methyl radicals may also abstract a terminal methyl hydrogen from m-xylene to form stable methylbenzyl radicals. The large excess of

10.1021/jp8020003
Published on Web 07/10/2008

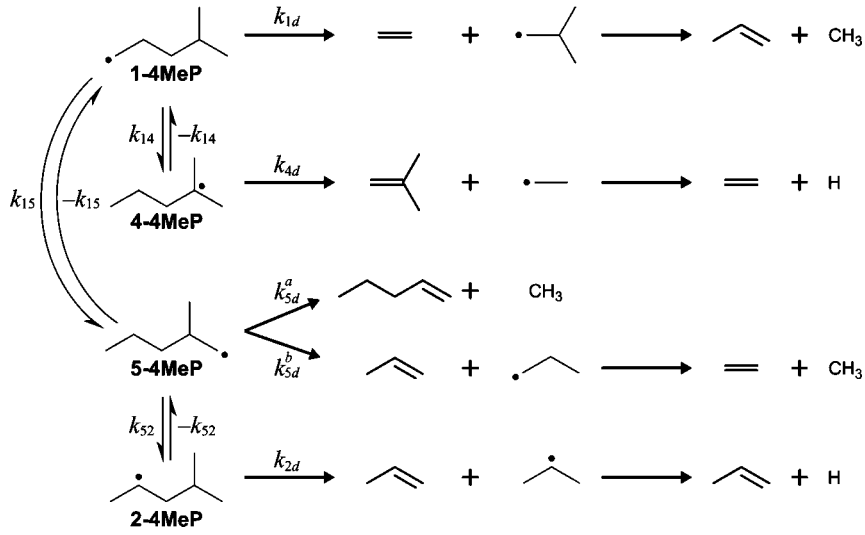

Figure 1. Decomposition mechanism for 4-methyl-1-pentyl radical. Secondary decomposition of the short-chain radical products produces additional olefin products, as shown on the right side of the figure.

scavenger ensures that the olefin products are derived solely from unimolecular decomposition reactions of 4-methylpentyl radical isomers.

The reaction temperature was determined by monitoring the reaction of chlorocyclohexane to form HCl and cyclohexene. The known[11] rate expression for chlorocyclohexane decomposition, $k = 10^{13.8} \exp(-25\,200/T)\ s^{-1}$, was used to calculate the overall temperature from the measured extent of reaction. Under the conditions of the present work, the short-chain radicals formed from the decomposition of each C_6 radical isomer further decompose to form an olefin and either methyl or H radicals (see Figure 1).

4-Methyl-1-pentyl radicals were generated from the shock heating of 1-iodo-4-methylpentane. The primary reaction that occurs at the temperatures of the present study is dissociation of the C−I bond to form the 4-methyl-1-pentyl radical. Molecular elimination of HI to form 4-methyl-1-pentene was also observed but does not impact our analysis of the radical decomposition and isomerization channels.

Results

Experiments were performed in the temperature range 927−1068 K with a corresponding pressure range of 1.78−2.44 bar. Major stable products of the decomposition of 1-iodo-4-methylpentane were ethene, propene, 2-methylpropene (isobutene), 1-pentene, and 4-methyl-1-pentene. The formation of 4-methyl-1-pentene is derived from molecular elimination of HI with a rate constant $k_{HI} = 10^{10.5} \exp(-18\,400/T)\ s^{-1}$. The corresponding C−I dissociation rate constant, determined from the difference between the disappearance of reactant and appearance of 4-methyl-1-pentene, was found to be $k_{C-I} = 10^{13.8} \exp(-24\,500/T)\ s^{-1}$. At the highest temperatures in the present study, a minor decomposition channel from this product may be present, but the expected concentrations of the short-chain decomposition products, specifically allyl radicals and propene, will represent a negligible fraction of the measured product concentrations at the temperatures in the present study. It is not considered further in this work. Substantial concentrations of toluene and methane were also observed. These correspond to the reactions of H and CH_3 with the radical scavenger and indicate these radical species are formed during the course of the reaction. Shown in Figure 2 is the product spectrum for the four major olefinic products of unimolecular decomposition of the radical.

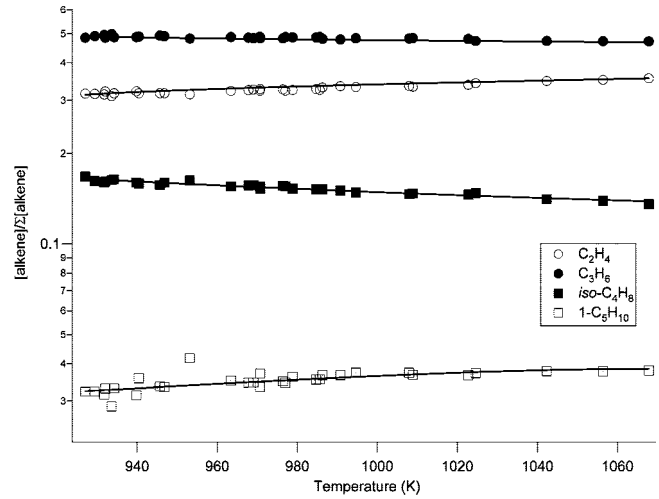

Figure 2. Product spectrum for the decomposition of 4-methyl-1-pentyl radical. Open circles, closed circles, closed squares, and open squares represent the relative concentrations of ethene, propene, 2-methylpropene (isobutene), and 1-pentene, respectively. Lines represent simultaneous fits from a kinetic model as discussed in the text.

The product spectrum is dominated by propene and ethene with smaller contributions from isobutene and 1-pentene. The decomposition mechanism, shown in Figure 1, has several pathways for the formation of ethene and propene, whereas isobutene and 1-pentene are formed from only single reaction channels. The short-chain C_2−C_4 radicals formed by decomposition of the C_6 radicals undergo secondary decomposition under the conditions of the present experiments to form olefins and CH_3 or H as shown. The isobutene product acts as a unique marker for the decomposition of 4-4MeP, and 1-pentene is unique to one of the two decomposition pathways for 5-4MeP. The decompositions of 1-4MeP and 5-4MeP, in the other of its two branches, lead to equal concentrations of propene and ethene. The observed excess of propene relative to ethene must therefore be derived from decomposition of 2-4MeP that occurs in excess of the decomposition of 4-4MeP.

The isomerizations shown in Figure 1 of 1-4MeP to form 4-4MeP and 5-4MeP occur through five- and six-membered cyclic transition states, respectively, and a secondary isomerization of 5-4MeP to 2-4MeP also occurs through a five-membered transition state. Isomerizations occurring through

TABLE 1: Rate Parameters in Arrhenius Form, $k = A \exp(-E_a/RT)$, derived from RRKM/ME Calculations at Three Temperatures and Pressures: 900 K, 1.71 bar; 1000 K, 2.19 bar; and 1100 K, 2.67 bar[a]

rate constant	reaction	$\log_{10} A$ (s^{-1})	E_a/R (K)
k_{1d}	1-4MeP → C_2H_4 + i-C_4H_9	11.30	11 140
k_{4d}	4-4MeP → i-C_4H_8 + C_2H_5	12.48	10 580
k^a_{5d}	5-4MeP → 1-C_5H_{10} + CH_3	11.36	11 770
k^b_{5d}	5-4MeP → C_3H_6 + n-C_3H_7	11.68	11 360
k_{2d}	2-4MeP → C_3H_6 + i-C_3H_7	12.46	10 615
k_{15}	1-4MeP → 5-4MeP	10.43	6555
$-k_{15}$	5-4MeP → 1-4MeP	10.28	6749
k_{14}	1-4MeP → 4-4MeP	10.11	7463
$-k_{14}$	4-4MeP → 1-4MeP	10.39	9303
k_{52}	5-4MeP → 2-4MeP	10.52	8449
$-k_{52}$	2-4MeP → 5-4MeP	11.12	9855

[a] These parameterizations do not represent elementary reaction rates at a single pressure. Rate constant identifiers are shown in Figure 1.

four-membered cyclic transition states, such as 1-4MeP ⇌ 3-4MeP and 2-4MeP ⇌ 4-4MeP (not shown in Figure 1), are expected to have substantially greater barriers to reaction due to ring strain in the transition states. Specifically, decomposition of 3-4MeP, which cannot be formed from a five-or six-membered transition state, would yield 3-methyl-1-butene, *E*-2-pentene, and *Z*-2-pentene through its β-bond scission pathways. These compounds were not observed from 100 ppm mixtures of the initial reactant down to the GC detection limit (~0.1 ppm). We have therefore assumed that isomerizations through four-membered transition states are unimportant in this system and consider only isomerizations occurring through five- and six-membered transition states.

Arrhenius parameters for the decomposition and isomerization reactions have been obtained by fitting the experimental data to a chemical kinetic model. The model includes the decomposition reactions of 1-4MeP, 2-4MeP, 4-4MeP, and 5-4MeP as well as the isomerization reactions between these various parent isomers. In addition, secondary decomposition reactions of the short-chain radical species formed from the parent decomposition have been incorporated. As observed previously,[4,12] the decomposition and isomerization reactions of alkyl radicals show a strong pressure-dependence at temperatures relevant to combustion, 500−1900 K. As such, the Arrhenius parameters obtained during direct fitting of the data in Figure 2 are valid only at the temperatures and pressures of the present study. In order to determine the high-pressure limiting Arrhenius parameters as well as the pressure-dependence of the rate constants, we have utilized the ChemRate software package[13] to perform RRKM/master equation (RRKM/ME) calculations.[3,14] After a discussion of the features of the chemical kinetic model utilized, the assumptions and inputs used in the RRKM/ME calculations will be detailed.

Kinetics Model

As illustrated in Figure 1, the two major types of reaction that the radical species undergo are decomposition and isomerization. Under the extremely low substrate concentrations (100 ppm) employed in the present experiments, the reverse reactions to the decompositions are unimportant; however, both the forward and reverse isomerization reactions must be considered. These reactions are shown in Table 1 with the kinetics parameters used in the final model (*vide infra*). Secondary decomposition reactions of the short-chain radicals to form alkenes and CH_3 or H and are shown in Table 2. The CH_3 and H products are assumed to react with the radical scavenger and are not considered further in the present study. Results from an RRKM/ME model calculation were used in the kinetics model to generate a product spectrum for comparison to the data in Figure 2. Thermodynamics and frequencies were adjusted in the RRKM/ME model to provide the best fit to the observed product concentrations. Details on the RRKM/ME calculations are provided below.

TABLE 2: Modified Arrhenius parameters, $k = A(T/298\ K)^n \exp(-E_a/RT)$, for Secondary Decomposition Reactions

reaction	$\log_{10} A$ (s^{-1})	n	E_a/R (K)	ref
i-C_4H_9 → C_3H_6 + CH_3	13.30		15 100	15
n-C_3H_7 → C_2H_4 + CH_3	13.08		15 200	16
i-C_3H_7 → C_3H_6 + H	13.20		18 000	16
C_2H_5 → C_2H_4 + H	20.38	−9.26	24 910	see text[a]
1-C_5H_{10} → C_3H_5 + C_2H_5	−34.04	45.52	−26 870	see text[a]

[a] Arrhenius parameters are only a parametrization and do not represent an elementary reaction rate.

The Arrhenius parameters for the secondary decompositions were taken from the literature and are shown in Table 2.[15,16] The reactions of n-C_3H_7, i-C_3H_7, and i-C_4H_9 are relatively fast at the present reaction temperature, with half-lives <15 μs at the lowest reaction temperature. However, at the lowest reaction temperatures, the decomposition of the ethyl radical, C_2H_5, is not necessarily complete in the 500 μs length of the shock and shows a significant pressure-dependence under these conditions. The parameters given in Table 2 for C_2H_5 decomposition are derived from a simple RRKM/ME model. Parameters were chosen for the reactant and transition state such that the calculated high-pressure limit matched the data of Baulch et al.[17] Assumptions and collisional treatments were similar to those used for the 4-MeP isomers (*vide infra*). Rate constants for the ethyl decomposition were calculated using ChemRate at six temperatures between 850 and 1150 K and their corresponding calculated postshock pressures, ranging from 1.50 to 2.66 bar. The resulting rate constants were parametrized using a modified Arrhenius expression and incorporated into the model. This correction changes the calculated relative concentrations by <5% relative to the assumption that ethyl radicals dissociate completely at all temperatures in the present study. However, its use is necessary to correctly model the slight curvature found in the lower temperature data shown in Figure 2.

A correction for the secondary decomposition of 1-pentene to form allyl and ethyl radicals was also used. The anticipated correction is small, and a complete study of 1-pentene dissociation is unwarranted for analysis of the present data. We have therefore elected to estimate the rate of this reaction based on shock tube data obtained in our laboratory on the decomposition of 1,8-nonadiene to form the allyl radical and 5-hexen-1-yl radical. This reaction is similar to the 1-pentene decomposition, in that allyl radicals are formed in conjunction with a primary radical having no additional resonance stabilization. The decomposition rate of 1,8-nonadiene is expected to be very similar to that of 1-pentene after correction by a factor of 2 to account for differences in the reaction degeneracy. Shock decomposition of 1,8-nonadiene in the presence of a large excess of radical inhibitor has a complex product spectrum, and a complete analysis will be the subject of a future publication. However, the disappearance rate is straightforwardly obtained from the measured product spectra, and a correction may be

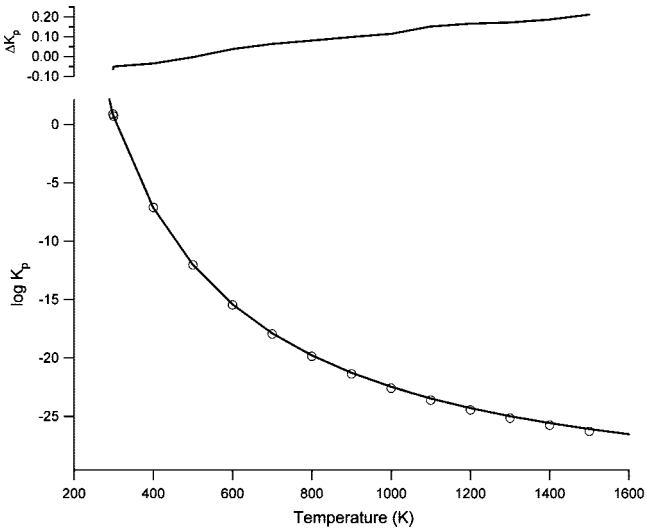

Figure 3. Equilibrium constant of formation, K_p, for 2-methylpentane. Open circles represent recommendations from ref 20, K_p^{API}. The line on the lower plot represents the equilibrium constant calculated from the thermodynamic model, K_p^{model}. The upper plot shows the residual difference, $\Delta K_p = K_p^{model} - K_p^{API}$, for the entire temperature range.

obtained. This correction changes the calculated 1-pentene concentration by <5% at the highest temperatures but is necessary to model the observed high-temperature curvature.

The expressions for the rate constants for ethyl radical and 1-pentene decomposition are shown in Table 2 are modified Arrhenius expressions that parametrize the rate constants over the specific temperatures and pressures of the present experiments. The values in the table should be treated only as parametrization corrections for the current data set and do not represent elementary reaction rates.

RRKM/Master Equation Modeling

Thermodynamics. The thermodynamics of the *x*-4MeP ($x = 1, 2, 4, 5$) radical reactant species have not been measured. Thermodynamic data for the reactant species were therefore determined based on a statistical thermodynamic model for the nonradical analogue of the reactants, 2-methylpentane. Vibrational partition functions were calculated using recommended frequencies from Benson.[18] The molecules were treated as pseudosymmetric top molecules wherein the idealized 2-dimensional moment of inertia was the geometric mean of the two largest moments of inertia of the molecule, and the idealized 1-dimensional rotor of the top was the smallest molecular moment. Rotational partition functions were calculated using hindered internal rotors with torsional barriers as recommended by Stull et al.[19] The vibrational frequencies in the 2-methylpentane statistical model were then adjusted to match the calculated model equilibrium constants of formation with the recommended values from the American Petroleum Institute (API) for temperatures from 298 to 1500 K.[20] The resulting fit is shown in Figure 3.

Thermodynamic models for the 1-, 2-, 4-, and 5-4MeP radicals were obtained by removing an appropriate H-atom. Standard enthalpies of formation were determined using assumed bond dissociation energies of 420, 410, and 403 kJ mol^{-1} for methyl, methylene, and methine C−H bonds, respectively, with the enthalpy of formation of 2-methylpentane taken from ref 20. Vibrational frequencies corresponding to C−H stretching and bending modes were removed or adjusted as suggested by Pitzer for the CH_3 and CH_2 moieties.[21] Since the H-atom mass is small relative to the molecule, no corrections to the overall external moments of inertia were made. However, the internal rotors were adjusted so that the rotors containing the radical centers were made free (no barrier to internal rotation) with correspondingly decreased moments of inertia. Expressions for the equilibrium constants of formation as used in the present analysis are shown in Table 3 as functions of temperature.

TABLE 3: Equilibrium Constants of Formation (K_f) for Reactant Radical Isomers[a]

radicals	$\log_{10} K_f$
1-4MeP	$-51.646 + 2.808 \ln T - 2.893 \times 10^{-4} T + 5614.3T^{-1} - 1.7465 \times 10^{6} T^{-2} + 1.9822 \times 10^{8} T^{-3} - 8.5425 \times 10^{9} T^{-4}$
2-4MeP	$-51.962 + 2.808 \ln T - 2.889 \times 10^{-4} T + 6267.7T^{-1} - 1.7828 \times 10^{6} T^{-2} + 2.0229 \times 10^{8} T^{-3} - 8.7150 \times 10^{9} T^{-4}$
4-4MeP	$-52.083 + 2.810 \ln T - 2.894 \times 10^{-4} T + 6490.7T^{-1} - 1.7397 \times 10^{6} T^{-2} + 1.9694 \times 10^{8} T^{-3} - 8.4790 \times 10^{9} T^{-4}$
5-4MeP	$-51.345 + 2.808 \ln T - 2.893 \times 10^{-4} T + 5614.3T^{-1} - 1.7465 \times 10^{6} T^{-2} + 1.9822 \times 10^{8} T^{-3} - 8.5425 \times 10^{9} T^{-4}$

[a] Temperature, *T*, in K.

Decomposition Reactions. Standard enthalpies of formation of the decomposition transition states were initially estimated from reverse reaction activation energies for similar reactions, as compiled by Kerr and Parsonage.[22] Appropriate activation barriers for these reverse reactions were determined by considering both the radical character (1°, 2°, and 3°) and the extent of substitution of the alkene, which in turn defines the radical character of the adduct. The decomposition transition state vibrational frequencies were determined by removing a single frequency from the reactant corresponding to the disappearing C−C stretch, representing the reaction coordinate. The internal rotors remained identical with the exception of freezing the free rotor corresponding to the reactant radical site (which becomes a double bond in the products) while allowing the rotor around the breaking bond to become free. The relative product spectrum, as shown in Figure 2, is sensitive to the relative decomposition and isomerization rates but is relatively insensitive to the absolute values. We have thus elected to fix the high-pressure limit Arrhenius parameters for β C−C bond fission in 1-4MeP to match those previously reported for 1-hexyl radical.[4] This was accomplished through slight adjustments of the transition state properties. With these fixed Arrhenius parameters, the low frequencies and enthalpies for the remaining decomposition reactions were slightly adjusted during the fitting procedure to best reproduce the measured product spectrum.

Isomerization Reactions. The isomerization reactions occur via hydrogen transfer reactions through cyclic transition states. As described above, we find no evidence for isomerization reactions occurring through four-membered transition states, and we assume that only five- and six-membered transition states are important. Three reaction pairs, 1-4MeP ⇌ 5-4MeP, 1-4MeP ⇌ 4-4MeP, and 5-4MeP ⇌ 2-4MeP, are therefore considered.

To model the transition states for H abstraction, we begin with the models for the reactant species and remove vibrational frequencies corresponding to the C−H stretches appropriate to the reaction coordinate. In the cyclic transition states for these reactions, hindered rotors in the linear species become low-frequency vibrations when they are part of the ring. For each isomerization reaction, appropriate hindered rotors were removed and replaced by 350 cm^{-1} vibrations as an initial guess for the transition state frequency spectrum. This frequency is an arbitrary choice but represents a reasonable estimate of the frequency of the C−C−C wagging modes induced by the cyclization of the molecule in the transition state. Internal rotors from the reactant that are not a part of the ring system in the

transition state remain unchanged. As in the case of the decomposition reactions, it is the relative and not absolute kinetics of the isomerization reactions that are of primary importance in fitting the data in Figure 2. We initially attempted to derive absolute values by fixing the Arrhenius parameters of the 5-4MeP → 2-4MeP isomerization to match those of the 1−3 isomerization in the *n*-hexyl radical. This is the only reaction in the decomposition of the methylpentyl radical for which a five- or six-membered transition state for isomerization from a primary to secondary radical is present. In principle, this isomerization is expected be very similar to the 1−3 isomerization of the *n*-hexyl radical, but we were unable to obtain a fit to the data with reasonable kinetics parameters with this constraint. Compared with the *n*-hexyl system, decreasing the activation energy for the 5−2 isomerization by 4.6 kJ mol^{-1} allowed a reasonable fit. As noted previously for the *n*-hexyl radical, tunneling in the H-atom transfer is important under these conditions, and we have elected to use a symmetric Eckart barrier with a width of 1.15 Å. This value is identical to that used in the previous study, and no attempt to optimize it further was made.

Collisional Energy Transfer and Chemical Activation. All experiments in the present study were performed in argon. Collisional energy transfer probabilities, $P(E,E')$, are treated with an exponential-down model:[23]

$$P(E,E') = \frac{1}{N(E')} \exp\left[-\left(\frac{E'-E}{\alpha}\right)\right] \quad (1)$$

where $N(E')$ is a normalization constant. In the present system, the collision of all reactant molecules with argon is treated with a constant $\alpha = 500$ cm^{-1}, a value typically used in treating pressure-dependent shock tube data.[3]

As discussed previously,[14] these reactions have low reaction thresholds with respect to the initial energy distributions of the reactant molecules. Such combinations of low thresholds with broad, high-energy reactant distributions are best treated as chemically activated systems. In our treatment, 1-iodo-4-methylpentane is assumed to produce a constant incoming flux of 4MeP radicals having a Boltzmann energy distribution corresponding to the reaction temperature. The evolution of the energy distributions of the reacting molecules thus reflects a competition between this incoming flux, the outgoing flux of reacting molecules with its dependence on the microcanonical reaction rate, and collisional energy transfer during the period of reaction.

Incorporation of RRKM/ME Results Into Kinetics Model. The RRKM/ME results were incorporated into the kinetics model by calculating the rate constants at three temperature−pressure pairs: 900 K, 1.71 bar; 1000 K, 2.19 bar; and 1100 K, 2.67 bar. These temperatures were chosen to bracket the range of experimental data. The pressures were calculated using standard shock expressions[24] under the conditions of the present experiment. These rate constants were then fit to an Arrhenius expression, which was used directly in the chemical kinetics model. The parameters at these three $T-P$ pairs for the best-fit model are shown in Table 1. Note that these expressions are only relevant under the conditions of the present experiment and are not suitable for more general modeling. High-pressure limit modified Arrhenius expressions derived from the partition functions of species in the best-fit RRKM/ME model are provided in Table 4. Pressure-dependent deviations from the high-pressure limit are shown in Table 5.

Traditional solutions[23,25] of the RRKM/ME problem assume that the rate constants become constant under particular temperature and pressure conditions with a very short induction time relative to the time scale of the reaction. As demonstrated previously,[3,14] this assumption does not necessarily hold under the peculiar combinations of high temperature and low reaction thresholds as are found in the present shock experiments and in typical combustion environments. Shown in Table 5 are the converged values of the ratio of the rate constant at the listed temperature and pressure to the high-pressure limiting rate constant ($k(T,P)/k_\infty$), irrespective of the length of the induction time. Unless otherwise noted, the calculated rate constants converged to within 5% of the final rate constants within an induction time of $<1 \times 10^{-5}$ s. Those cases where the time required for the rate constant to converge is longer than this time are noted in the table. The values of the induction times given in the table for those slowly converging combinations of temperature and pressure represent upper limits to the time required for convergence and are valid to within 1 order of magnitude. No attempt to determine more accurate induction times was made.

TABLE 4: High-Pressure Limit Modified Arrhenius Parameters, $k = A(T/298\ \text{K})^n \exp(-E_a/RT)$, for Reactions of 4-Methylpentyl Radical Isomers from 500 to 1900 K

rate constant	$\log_{10} A$ (s^{-1})	n	E_a/R (K)
k_{1d}	12.64	0.511	13 730
k_{4d}	13.23	0.675	12 370
k_{5d}^a	12.66	0.572	14 490
k_{5d}^b	12.97	0.498	13 990
k_{2d}	12.87	0.851	11 990
k_{15}	9.115	2.40	5955
$-k_{15}$	8.814	2.40	5955
k_{14}	8.719	2.62	6856
$-k_{14}$	9.121	2.60	8917
k_{52}	8.973	2.78	7781
$-k_{52}$	9.434	2.91	9009

Discussion

Distributions and Reaction Thresholds. The entries in Table 5 show generally larger deviations from the high-pressure limit as temperature increases at constant pressure, as expected for a pressure-dependent reaction rate. However, as similarly observed for the decomposition of the *n*-hexyl radical,[4] the trend inverts at higher temperatures and lower pressures. As illustrated below, this effect may be attributed to the time-dependence of the energy distributions of the various reactant species.

The induction time is the time required to obtain a stable rate constant at a given temperature and pressure. Traditionally, pressure-dependent reactions are treated as having a rate constant that is independent of time at a particular temperature and pressure. It is assumed that the time required to establish these invariant rates is short relative to the time scale of the reaction. However, in cases where reaction thresholds are much lower than the average energy of the reactant molecule, as is found in the present system at higher temperatures, the induction times may be comparable to the characteristic reaction times.[3,14] Under these conditions, the apparent reaction rates and thus the branching ratios will be poorly modeled by an RRKM/ME analysis that provides a single time-independent rate constant for each reaction.

The changes in these energy distributions over time for the 1-4MeP, 2-4MeP, and 5-4MeP isomers at 1500 K and 0.1 bar are shown in Figure 4, where a Boltzmann distribution at 1500 K is illustrated by the shaded area. For 1-4MeP, the initial radical formed in the present system, a Boltzmann distribution of initial energies is assumed, as discussed above, and the distribution at

TABLE 5: Deviations from the High-Pressure Limit after Induction Period, $k(T, P)/k_\infty(T)$[a]

		temperature (K)							
reaction	P (bar)	500	700	900	1100	1300	1500	1700	1900
k_{1d}	0.1	0.94[b]	0.48[c]	0.12	0.05	0.05	0.06	0.09	0.14
	1	0.99	0.84	0.40	0.16	0.11	0.11	0.13	0.17
	10	1.00	0.98	0.78	0.44	0.26	0.20	0.20	0.22
	100	1.00	1.00	0.97	0.82	0.58	0.42	0.35	0.32
	1000	1.00	1.00	1.00	0.98	0.90	0.77	0.63	0.54
k_{4d}	0.1	0.94[d]	0.63[c]	0.25	0.10	0.07	0.06	0.08	0.12
	1	0.99[b]	0.88	0.57	0.28	0.17	0.13	0.14	0.17
	10	1.00[c]	0.97	0.86	0.61	0.38	0.27	0.24	0.25
	100	1.00	1.00	0.98	0.90	0.72	0.54	0.44	0.39
	1000	1.00	1.00	1.00	1.00	0.96	0.87	0.74	0.64
k_{5d}^a	0.1	0.96[b]	0.52	0.14	0.04	0.03	0.03	0.03	0.04
	1	1.01[c]	0.89	0.47	0.17	0.08	0.06	0.06	0.07
	10	1.01[c]	1.00	0.85	0.50	0.26	0.16	0.12	0.12
	100	1.01	1.01	0.99	0.86	0.63	0.42	0.30	0.24
	1000	1.01	1.01	1.01	0.97	0.91	0.80	0.64	0.51
k_{5d}^b	0.1	0.95[b]	0.54	0.15	0.05	0.03	0.03	0.03	0.05
	1	0.99[c]	0.89	0.49	0.19	0.09	0.06	0.06	0.07
	10	0.99[c]	0.98	0.85	0.53	0.28	0.17	0.13	0.13
	100	1.00	0.99	0.97	0.87	0.64	0.44	0.31	0.25
	1000	1.00	1.00	0.99	0.98	0.92	0.80	0.65	0.52
k_{2d}	0.1	0.98[b]	0.70[c]	0.28	0.10	0.05	0.04	0.04	0.04
	1	1.01[b]	0.92	0.63	0.31	0.15	0.10	0.08	0.08
	10	1.01[c]	1.00	0.91	0.66	0.40	0.25	0.18	0.16
	100	1.01	1.01	1.00	0.93	0.76	0.56	0.41	0.33
	1000	1.01	1.02	1.01	1.00	0.97	0.89	0.76	0.63
k_{15}	0.1	1.00	0.81	0.41	0.22	0.16	0.15	0.17	0.22
	1	1.00	0.96	0.69	0.41	0.28	0.23	0.23	0.26
	10	1.00	1.00	0.92	0.68	0.48	0.36	0.33	0.33
	100	1.00	1.00	0.99	0.92	0.75	0.58	0.49	0.44
	1000	1.00	1.00	1.00	1.00	0.96	0.83	0.72	0.64
$-k_{15}$	0.1	1.00[c]	0.91	0.53	0.27	0.16	0.11	0.10	0.11
	1	1.00	0.99	0.81	0.50	0.30	0.21	0.17	0.16
	10	1.00	1.00	0.97	0.79	0.55	0.37	0.29	0.25
	100	1.00	1.00	1.00	0.97	0.83	0.63	0.50	0.41
	1000	1.00	1.00	1.00	1.01	0.98	0.88	0.77	0.66
k_{14}	0.1	0.96	0.74	0.31	0.16	0.12	0.12	0.14	0.19
	1	0.97	0.93	0.61	0.34	0.22	0.19	0.20	0.23
	10	0.97	0.97	0.87	0.63	0.42	0.32	0.29	0.29
	100	0.97	0.98	0.97	0.91	0.72	0.55	0.45	0.41
	1000	0.97	0.98	0.98	1.01	0.95	0.84	0.71	0.62
$-k_{14}$	0.1	0.97[b]	0.72[c]	0.31	0.13	0.08	0.07	0.08	0.12
	1	0.99[b]	0.91	0.62	0.31	0.18	0.14	0.14	0.17
	10	1.00[c]	0.98	0.88	0.63	0.40	0.28	0.24	0.24
	100	1.00	1.00	0.98	0.91	0.73	0.54	0.43	0.38
	1000	1.00	1.00	1.00	0.99	0.96	0.87	0.74	0.63
k_{52}	0.1	0.96[c]	0.81	0.37	0.16	0.09	0.07	0.06	0.08
	1	0.96[c]	0.95	0.70	0.38	0.21	0.13	0.11	0.12
	10	0.96	0.97	0.92	0.72	0.45	0.28	0.22	0.19
	100	0.96	0.98	0.97	0.96	0.78	0.56	0.42	0.34
	1000	0.96	0.98	0.98	1.03	0.98	0.86	0.73	0.61
$-k_{52}$	0.1	0.99[b]	0.79[c]	0.37	0.14	0.07	0.05	0.04	0.05
	1	1.00[b]	0.95	0.69	0.37	0.18	0.11	0.09	0.09
	10	1.00[c]	0.99	0.92	0.71	0.44	0.27	0.20	0.17
	100	1.00	1.00	0.99	0.95	0.79	0.58	0.43	0.34
	1000	1.00	1.00	1.00	1.02	0.99	0.91	0.78	0.64

[a] The induction period, τ, is $<1 \times 10^{-5}$ s unless otherwise noted and represents the time at which the rate constant is within 5% of the rate constant at $t = \infty$. [b] $\tau < 0.001$ s. [c] $\tau < 0.0001$ s. [d] $\tau < 0.01$ s.

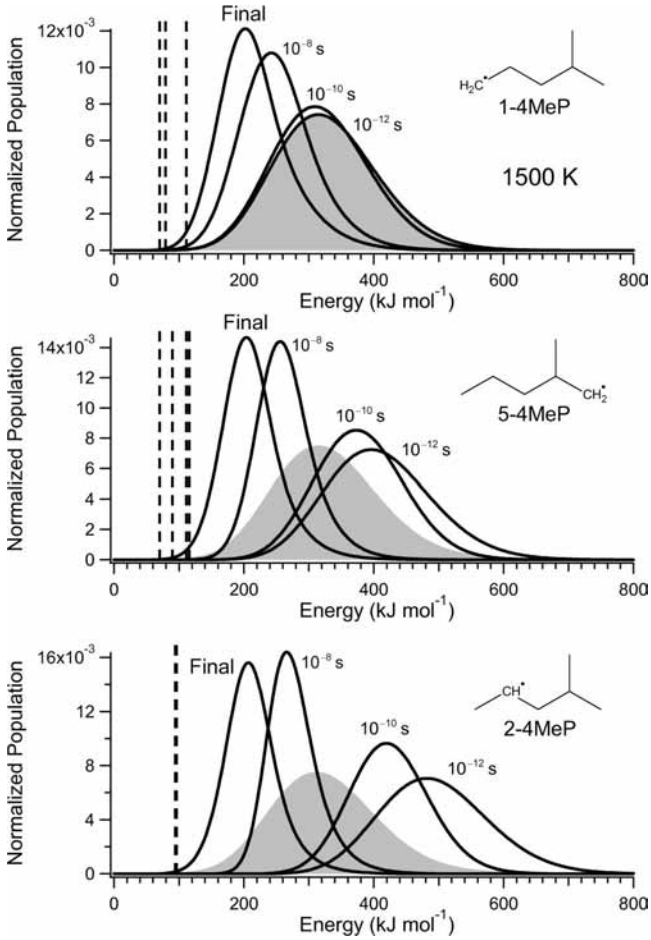

Figure 4. Normalized energy distributions as a function of time for 4-methylpentyl radical isomers derived from the reaction of 4-methyl-1-pentyl radical at 1500 K and 0.1 bar pressure. Dashed vertical lines represent thresholds for the various reactions of the isomer. The gray area is the Boltzmann energy distribution for the given isomer at 1500 K.

early times reflects this assumption. Since essentially the entire distribution lies above the reaction thresholds, all molecules undergo decomposition and isomerization reactions as shown in Figure 1. Also, the system undergoes collisions with the bath gas, argon in the present system, which drive the system toward the Boltzmann distribution. The resulting final distribution for the "steady-state" between the reactive disappearance of 1-4MeP and the collisional energy transfer is lower in energy than the initial distribution but still lies above the reaction thresholds. A rate constant derived from the steady-state value would substantially underestimate the true reaction rate at early times. The induction time noted in Table 5 is the time at which the chemical reactions and collisional stabilization have reached equilibrium and the "Final" distribution in Figure 4 has been established.

The distributions of the 5-4MeP isomer, which is formed from isomerization of 1-4MeP, show similar behavior, but the early time distributions are at higher energies because of chemical activation derived from reaction over a 68 kJ mol^{-1} barrier. At early times, the reactions proceed faster than comparable reactions in the 1-4MeP parent. Similarly, the short-time energy distributions of 2-4MeP, which are formed by isomerization of the 5-4MeP molecule, occur at higher energy because of the presence of an 87 kJ mol^{-1} barrier to reaction. At temperatures where the reaction rates are comparable to or greater than the collisional energy transfer rate, a significant fraction of 2-4MeP and 5-4MeP isomers will react during the induction time, and the rates of these reactions will be higher than expected from a steady-state RRKM/ME analysis. This effect is particularly prevalent in the isomerization reactions, since the relative rates depend strongly on the differences in the initial energy distributions of the reactive isomers. In these cases, the branching ratios will depend strongly on time, and a "steady-state" analysis is inappropriate for accurate modeling.

By definition, the high-pressure limiting rate represents the reaction rate of a species with a Boltzmann energy distribution, shown as a shaded area in the figure. Reactions of species with the "Final" distribution, which is lower in energy, will necessarily be slower than reactions of species with the Boltzmann distribution. In general, collisions force the distribution toward the Boltzmann distribution, while chemical reactions force the distribution toward the reaction thresholds, and the "Final" distribution is the equilibrium point between these extremes. At extremely high pressures, the energy distribution is entirely Boltzmann; as pressures decrease, the energy distribution shifts toward lower energies, and the effective reaction rate decreases. This shift manifests itself as the traditional falloff curve. As expected, the rate calculations show a pressure-dependent falloff at constant temperature for all reactions shown in Table 5.

In general, at a constant pressure, one would expect a larger deviation from the high-pressure limit as temperature increases, because the Boltzmann distribution shifts to higher energies with correspondingly increased microcanonical reaction rates. The collisional energy transfer rates, which do not increase as rapidly as the reaction rates with increasing temperature, become less competetive with increasing temperatures. At the lower temperatures and higher pressures shown in Table 5, this trend is observed, but at the higher temperature and lower pressures the trend reverses. The ratio k/k_∞, where k_∞ represents the high-pressure limit, begins to go back toward unity with increasing temperature at constant pressure. At the highest temperatures shown in the table, the reaction rates are such that the extent of reaction is significant during the length of the induction time. During this time, the energy distributions are higher in energy than the "steady-state" distribution and are closer to those of the Boltzmann distribution, yielding an effective reaction rate closer to the high-pressure limit. Lower temperature reactions occur with much lower extents of reaction during the induction period, and the majority of reaction products are derived from reaction at energies near the steady-state distribution. At sufficiently high temperatures and low pressures, the observed rate constant will be higher than the high-pressure limit, since virtually all of the parent radicals have reacted prior to collisional energy stabilization to the Boltzmann distribution.[14]

To test the dependence of the calculated reaction thresholds and pressure-dependent rate constants, calculations were performed with a exponential-down decay parameter (eq 1) of $\alpha = 300$ cm^{-1}. Since the current experimental data lie in the falloff region, this parameter is expected to impact the calculated reaction thresholds in addition to the pressure-dependence. We find that acceptable fits may be obtained by changing the isomerization reaction thresholds by no more than ± 1.0 kJ/mol; however, the calculated deviations from the high-pressure limit (k/k_∞) differ more strongly from unity with $\alpha = 300$ cm^{-1} than with $\alpha = 500$ cm^{-1} as shown in Table 5. Calculated high-pressure limiting rate expressions and time- and pressure-dependent rate constants may be found in the Supporting Information with $\alpha = 300$ cm^{-1}.

SCHEME 1: Decomposition of Straight-Chain and Branched Primary Radicals

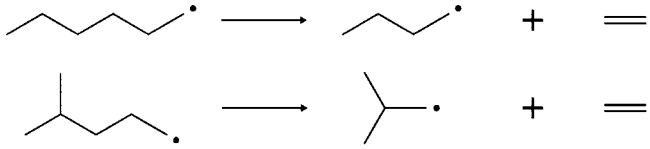

SCHEME 2: Decomposition of Straight-Chain and Branched Secondary Radicals

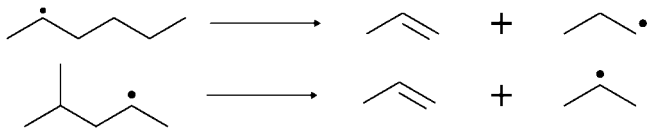

SCHEME 3: Decomposition of Radicals Occurring via Multiple Pathways

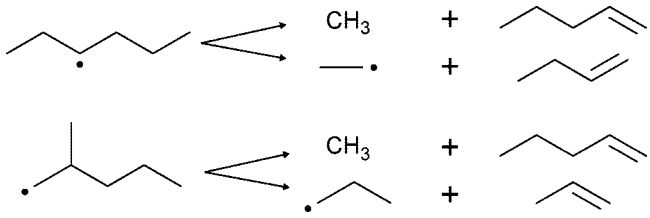

Effects of Methyl Substitution. ***Decomposition Reactions.*** Several of the reaction rates in the present system have analogues in the pyrolysis of *n*-hexyl radical previously described in our laboratory.[4] Decomposition of 1-4MeP to form C_2H_4 and isobutyl radical should have a rate constant of decomposition essentially identical to that of the decomposition of 1-hexyl radical to form C_2H_4 and 1-butyl radical (Scheme 1). As discussed above, we have fixed the absolute 1-4MeP decomposition rate to be identical to the 1-hexyl decomposition rate in the fits.

The β-bond scission of 2-4MeP, which yields propene and secondary propyl radical, is analogous to the decomposition of 2-hexyl to form propene and *n*-propyl as shown in Scheme 2. However, the rate of 2-4MeP decomposition is found to be higher than that of 2-hexyl by a factor of 7.6 at 1000 K. This difference is due to a lower activation energy for the formation of the secondary isopropyl radical relative to the primary *n*-propyl radical, as the preexponential factors for these reactions are similar.

The decomposition of 4-4MeP, which produces a secondary alkene (isobutene) and a primary radical (ethyl), has no obvious analogue in *n*-hexyl radical decomposition. This decomposition shows comparable preexponential factors to those in the decomposition reactions of *n*-hexyl but has a lower activation energy, presumably due to the formation of the substituted alkene in the 4-4MeP system as opposed to the primary alkenes formed in the reactions of *n*-hexyl.

The decomposition of 5-4MeP occurs through two channels in a manner similar to that of 3-hexyl radical. As illustrated in Scheme 3, 3-hexyl radicals decompose to form 1-pentene and CH_3 (C5+C1) or 1-butene and C_2H_5 (C4+C2), whereas the 5-4MeP system decomposes to form either 1-pentene and CH_3 (C5+C1) or propene and n-C_3H_7 (C3+C3). The 5-4MeP is a primary radical as compared to the secondary 3-hexyl radical, which would tend toward lower activation energies for the 5-4MeP decomposition. However, the reactions corresponding to the reverse addition of the short-chain radical to the primary alkene to form the 3-hexyl and 5-4MeP radicals differ. In the formation of 3-hexyl, both CH_3 and C_2H_5 add terminally to their respective alkenes. The corresponding addition reactions occur on the nonterminal carbons in the formation of 5-4MeP, and larger barriers to reaction are therefore expected.[22] These two effects largely cancel, and we find that the rate constants differ by ~20% for the two systems at 1000 K. The ratios of rate constants between the decomposition of 5-4MeP and 3-hexyl radicals are similar at 1000 K with values of k(C3+C3)/k(C5+C1) = 3.07 and k(C4+C2)/k(C5+C1) = 2.92, respectively.

SCHEME 4: Isomerization through Six-Membered Transition States

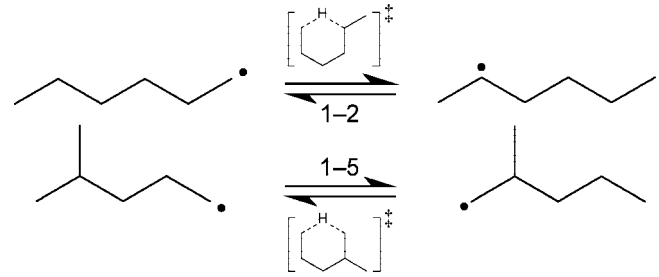

Isomerizations Through Hydrogen Transfer. The isomerization reactions of 1-4MeP also show some differences in reaction rates relative to those in *n*-hexyl radical. Of the isomerization reactions in the 4-MeP and hexyl radical system, only the 5-4MeP → 2-4MeP is identical to an analogous reaction in *n*-hexyl, 1-hexyl → 3-hexyl, in terms of the number of abstractable hydrogen atoms and the number of atoms involved in the transition state. Both of these isomerizations occur via a five-membered transition state from a primary radical parent by abstracting a methylene hydrogen atom. As discussed above, we have assumed that these reactions have similar absolute rate constants and allowed all of the other reaction rate constants to float in the fitting of the product spectrum.

The only observable isomerization reactions that occur via six-membered transition states are the 1-4MeP ⇌ 5-4MeP in the present system and the 1-hexyl ⇌ 2-hexyl in *n*-hexyl radical decomposition (Scheme 4). The observed activation energy for the 1−5 isomerization is higher than that for the corresponding 1−2 isomerization in *n*-hexyl radical, as expected due to the thermochemistry of the primary−primary radical conversion. Since there are six abstractable methyl hydrogen atoms in the 1-4MeP → 5-4MeP conversion compared to two methylene hydrogen atoms in the 1-hexyl → 2-hexyl system, the A-factors are expected to differ by a factor of ~3; the observed ratio derived from the fits is 3.25−2.74 from 500 to 1500 K. As expected, the reverse 5−1 isomerization of 5-MeP has a substantially lower activation energy than the corresponding 2−1 isomerization of 2-hexyl radical.

The 1−4 isomerization of 4MeP radical occurs via a five-membered transition state similar to the 1−3 isomerization in *n*-hexyl radical (Scheme 5). The presence of a single abstractable methine hydrogen in 1-4MeP is expected to have a significant effect on the observed relative A-factors; at 1000 K, the ratio of A-factors was found to be 0.45. The formation of the tertiary product tends to yield a lower activation energy, and the activation energy was found to be lower in the 1−4 isomerization of 4MeP. Overall, the isomerization rate for the 1−4 isomerization was found to be a factor of 2.0 faster at 1000 K than the 1−3 isomerization of *n*-hexyl radical, yielding a factor of 4.0 increase in the rate on a per-hydrogen basis, due to the differences in the number of abstractable hydrogen atoms in the two systems.

SCHEME 5: Isomerization through Five-Membered Transition States

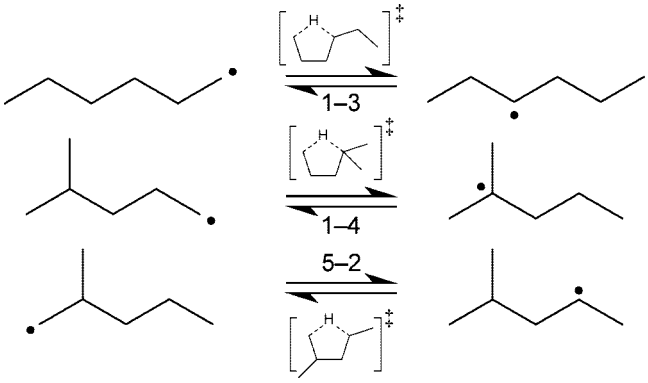

Pressure-Dependence. The pressure-dependence of the reaction rates relative to the high-pressure limit are similar in the analogous reactions between 4MeP and *n*-hexyl with devations generally tending to deviate less from unity in the present system. The pressure-dependence of the nonanalogous reactions, namely those involving the tertiary 4-4MeP radical or the decomposition of 2-4MeP to form a secondary radical, is slightly different, especially at lower temperatures. In both of these systems, the decomposition reactions show a weaker pressure-dependence relative to that of the other decomposition reactions. The isomerization reactions involving the 4-4MeP, however, show a slightly stronger pressure-dependence, especially at lower temperatures. In both the decomposition and isomerization reactions, the pressure-dependences are similar for all reactions at higher temperature. At lower temperatures, the differences between these reactions are larger, but the absolute deviations from the high-pressure limit lie much closer to unity. In general, the addition of a branched moiety does not appear to have a strong effect on the calculated pressure-dependence.

Use in Combustion Mechanisms and Future Goals. The direct application of the present results in a combustion mechanism is complicated by several factors. First, 1-4MeP is not a common radical species in a typical combustion environment. Decomposition of a larger species, such as 2,2,6-trimethylheptane → *t*-butyl + 1-4MeP, would produce an appropriate radical species, but the 1-4MeP would not necessarily start at the bath temperature due to chemical activation in the decomposition.

Generalization of these results may be accomplished by considering the effects of the formation of radicals and alkenes at different levels of substitution combined with consideration of the number of abstractable hydrogen atoms in a given system. The results shown in Tables 4 and 5 may be parametrized for use in a chemical model with a few caveats. The results in Table 5 represent the fractional deviations from the high-pressure limits for each of the reactions in the decomposition mechanism at the stated temperature and pressure. These deviations are given in the long-time limit, irrespective of the induction time. Unless otherwise noted, the deviations at 1×10^{-5} s are within 5% of the reported values. However, particularly at lower temperatures and pressures, the deviations may require longer to stabilize, yielding a substantial fraction of the reactions of the radical species with rates that may differ markedly from those predicted from the tables. In cases where the reaction rates are faster than the anticipated induction times, calculation of the rate parameters, under conditions appropriate to the system being modeled, will be necessary. Similar calculations under conditions where 2-4MeP, 4-4MeP, and 5-4MeP are the initial radicals have been performed and are available in the Supporting Information.

Experiments on the decomposition of 5-methyl-1-iodohexane are currently underway to study the effects of the formation of a tertiary radical species via a six-membered transition state (5-methyl-1-hexyl ⇌ 2-methyl-2-hexyl).[26] These experiments, in addition to those reported presently, will provide insight into the overall isomerization mechanisms for decomposition and isomerization of branched hydrocarbon species and will ultimately lead to a greater understanding of the pyrolysis of branched paraffin systems.

Conclusion

The kinetics of the unimolecular reactions of 4-methyl-1-pentyl radical have been examined using a single-pulse shock tube with gas chromatographic detection from temperatures 927−1068 K and 1.78−2.44 bar pressure. Major products observed were propene, ethene, 2-methylpropene, and 1-pentene. Decomposition rates were generally found to be larger than those in the decomposition of unbranched alkyl radicals when substituted alkenes or secondary radicals were formed. Isomerization via H transfer rates were found generally to be faster due to the differences in thermochemistry between the branched and unbranched radical species as well as the number of hydrogen atoms participating in the isomerization. These data were used to validate a chemical model of the pressure-dependence, as manifested through the deviation from the high-pressure limit. Generally, the pressure-dependence was found to be weaker in the branched system than in the unbranched radical. Future experiments are underway to further examine the effects of branching on the rates of other similar reactions important in hydrocarbon pyrolysis.

Acknowledgment. This research was supported by the U.S. Department of Defense through the Strategic Environmental and Development Program (SERDP PP1198), Charles Pellerin, Scientific Officer.

Supporting Information Available: Raw alkene yields from the decomposition of 4-methyl-1-pentyl, shown in Figure 2; calculated pressure- and temperature-dependent deviations from the high-pressure limit with $\alpha = 300$ cm^{-1} (eq 1); deviations from the high-pressure limit for 2-4MeP, 4-4MeP, and 5-4MeP; and parameters used to model the reactant radical species. This material is available free of charge via the Internet at http://pubs.acs.org.

References and Notes

(1) Edwards, T.; Harrison,W. E., III; Maurice, L. Q. *Properties and Usage of Air Force Fuel: JP-8*, Proceedings of the 39th AIAA Aerospace Sciences Meeting and Exhibit, Reno, NV, Jan 8−11, 2001, AIAA 2001-0498.

(2) Richter, H.; Howard, J. B. *Prog. Energy Combust. Sci.* **2000**, *26*, 565–608.

(3) Tsang, W.; Bedanov, V.; Zachariah, M. R. *Ber. Bunsen−Ges.* **1997**, *101*, 491–499.

(4) Tsang, W.; Walker, J. A.; Manion, J. A. *Proceedings of the Combustion Institute*; 2007, Vol. 31, pp 141−148.

(5) Certain commercial materials and equipment are identified in this paper in order to specify adequately the experimental procedure. In no case does such identification imply recommendation or endorsement by the National Institute of Standards and Technology, nor does it imply that the material or equipment is necessarily the best available for the purpose.

(6) Tsang, W. In *Shock Waves in Chemistry*; Lifshitz, A., Ed.; Marcel Dekker: New York, 1981.

(7) Herzler, J.; Manion, J. A.; Tsang, W. *Int. J. Chem. Kinet.* **2001**, *33*, 755–767.

(8) McGivern, W. S.; Manion, J. A.; Tsang, W. *J. Phys. Chem. A* **2006**, *110*, 12822–12831.

(9) Robaugh, D.; Tsang, W. *J. Phys. Chem.* **1986**, *90*, 4159–4163.

(10) Manion, J. A.; Tsang, W. *J. Phys. Chem.* **1996**, *100*, 7060–7065.

(11) Benson, S. W.; O'Neal, H. E. *Kinetic Data on Gas Phase Unimolecular Reactions*; United States Department of Commerce: Washington, DC, 1970.

(12) Knyazev, V. D.; Slagle, I. R. *J. Phys. Chem.* **1996**, *100*, 5318–5328.

(13) Mokrushin, V.; Bedanov, V.; Tsang, W.; Zachariah, M.; Knyazev, V. *ChemRate*, version 1.5.4; National Institute of Standards and Technology: Gaithersburg, MD, 2006.

(14) Tsang, W.; Bedanov, V.; Zachariah, M. R. *J. Phys. Chem.* **1996**, *100*, 4011–4018.

(15) Tsang, W. *J. Phys. Chem. Ref. Data* **1990**, *19*, 1–68.

(16) Tsang, W. *J. Phys. Chem. Ref. Data* **1988**, *17*, 887–952.

(17) Baulch, D. L.; Cobos, C. J.; Cox, R. A.; Frank, P.; Hayman, G.; Just, T.; Kerr, J. A.; Murrells, T.; Pilling, M. J.; Troe, J.; Walker, R. W.; Warnatz, J. *J. Phys. Chem. Ref. Data* **1994**, *23*, 847–1033.

(18) Benson, S. W. *Thermochemical Kinetics: Methods for the Estimation of Thermochemical Data and Rate Parameters*; John Wiley & Sons: New York, 1968.

(19) Stull, D. R.; Westrum, E. F., Jr.; Sinke, G. C. *The Chemical Thermodynamics of Organic Compounds*; John Wiley & Sons: New York, 1969.

(20) Rossini, F. D.; Pitzer, K. S.; Arnett, R. L.; Braun, R. M.; Pimentel, G. C. *Selected Values of Physical and Thermodynamic Properties of Hydrocarbons and Related Compounds*; Volume *44* of American Petroleum Institute Research Project; Carnegie Press: Pittsburgh, PA, 1953.

(21) Pitzer, K. S. *J. Chem. Phys.* **1944**, *12*, 310–314.

(22) Kerr, J. A.; Parsonage, M. J. *Evaluated Kinetic Data on Gas Phase Addition Reactions: Reactions of Atoms and Radicals with Alkenes, Alkynes and Aromatic Compounds*; CRC Press: Cleveland, OH, 1972.

(23) Gilbert, R. G.; Smith, S. C. *Theory of Unimolecular and Recombination Reactions*; Blackwell Scientific: Oxford, 1990.

(24) Gaydon, A. G.; Hurle, I. R. *The Shock Tube in High-Temperature Chemical Physics*; Reinhold Publishing: New York, 1963.

(25) Holbrook, K. A.; Pilling, M. J.; Robertson, S. H. *Unimolecular Reactions*, 2nd ed.; John Wiley & Sons: New York, 1996.

(26) Awan, I. A.; McGivern, W. S.; Manion, J. A.; Tsang, W. Manuscript in preparation.

JP8020003